Ecological Indicators 154 (2023) 110704

Contents lists available at ScienceDirect

Ecological Indicators

journal homepage: www.elsevier.com/locate/ecolind

Accelerated vegetative growth measured by gross primary productivity in China from 1980 to 2018

Chan Zuo [a,b], Junbang Wang [a,*], Xiujuan Zhang [b], Alan E. Watson [c]

[a] National Ecosystem Science Data Center, Key Laboratory of Ecosystem Network Observation and Modeling, Institute of Geographic Sciences and Natural Resources Research, Chinese Academy of Sciences, Beijing 100101, China
[b] College of Horticulture and Gardening, Yangtze University, Jingzhou 434023, China
[c] USDA Forest Service, Rocky Mountain Research Station, Missoula, MT 59801, USA

ARTICLE INFO

Keywords:
Gross primary productivity
Periodic oscillations
Long-term trend
Vegetation response
Climate impacts

ABSTRACT

Vegetation response to climate change can be characterized as long-term trends, but with periodic oscillations. Revealing vegetation response trends, with oscillations, is essential for formulating climate change mitigation and adaptation planning, as well as adopting ecological protection and restoration measures. Here, the long-term trend and periodic oscillations in vegetation changes were explored through a measure of gross primary production (GPP), an indicator of vegetation photosynthesis, using data of both high spatial resolution (1 km^2) and a long-term of nearly 4 decades, from 1980 to 2018. The GPP data were estimated for China's terrestrial ecosystem and validated against the eddy covariance-based observations of 70 site-year in China and compared to other GPP data products. The results showed the estimated GPP can explain 76% of spatial–temporal variance with the same data accuracy as other products, but with the advantage of both high spatial resolution and long time periods that other products do not have. From the estimated GPP data, Chinese terrestrial vegetation growth was found to have a periodic oscillation of close to 2.79 years and a long-term increasing trend of 59.8 Mt C m^{-2} per ten years over 92% of all vegetated land in China from 1980 to 2018. Moreover, it was found that vegetation growth accelerated significantly in the two recent decades over the previous two decades. The growth rate was 83.5 Mt C a^{-1} from 2000 to 2018, which was 2.31 times faster than the rate from 1980 to 2000. The underlying mechanism of the vegetation responses was analyzed by ridge regression, a method to decrease the effects of multicollinearity. Long-term variability and trends in vegetation could be attributed to a warming minimum air temperature when examined with precipitation, maximum air temperature, and solar shortwave radiation. Though more influences, such as those from freezing and thawing and human activities, should be explored in the future, this study offers insight that warming, with increasing daily minimum temperatures, is likely to be a vital contributor to ecosystem changes, and will be essential knowledge for mitigation of effects and adaptation to future climate.

1. Introduction

It is essential to recognize and understand the response of vegetation to climate change in the past at multiple time scales for predicting changes in vegetation under future climate scenarios (Cramer et al., 2001; Fang et al., 2001; Li et al., 2018; Yuan et al., 2010). Changes in vegetation can be used to detect variability in bioclimatic processes at different temporal scales (Jing et al., 2021; Yin et al., 2017; Zhu et al., 2022). Gross Primary Productivity (GPP) is the total amount of organic during photosynthesis and can serve as the fundamental indicator of maintenance of terrestrial ecosystem services and sustainable development of human socio-economic systems (Anav et al., 2015; Beer et al., 2010; Damm et al., 2015). Influences on GPP are very important to understanding future vegetation variability and underlying mechanisms in the field of terrestrial ecosystem ecology and global change research, especially under the uncertainties associated with global climate change. (Gang et al., 2017; Xin et al., 2020).

Interannual changes in GPP have mostly been studied in relation to long-term trends, variability and extreme events of climate scenarios (Jiao et al., 2018; Lehouerou, 1984; Stephen et al., 2008; Zhu et al., 2021). Increasingly, long-term trends for GPP are believed to be influenced mainly by a warming climate (Chen et al., 2021; Nima et al.,

* Corresponding author at: A11, Datun Road, Chaoyang District, Beijing 10010, China.
E-mail address: jbwang@igsnrr.ac.cn (J. Wang).

https://doi.org/10.1016/j.ecolind.2023.110704
Received 18 September 2022; Received in revised form 7 July 2023; Accepted 19 July 2023
Available online 23 July 2023

2020). Some studies have found a negative effect of climate changes on GPP, with increased atmospheric vapor pressure deficit resulting in decreasing GPP (Ballantyne et al., 2017; Li, 2021; Nima et al., 2020; Yuan et al., 2019). The interannual variability of GPP and its underlying mechanisms have been uncertain to a great extent, with periodic oscillation of the interannual changes receiving little attention.

The Ensemble Empirical Mode Decomposition (EEMD) algorithm is an adaptive and noise-assisted time series analysis method widely used in signal processing, research on climate change and hydrologic processes. EEMD is an improvement over the Empirical Mode Decomposition (EMD) algorithm, which is a signal time–frequency processing method based on the Hilbert-Huang transformation (Huang et al., 1998; Wu and Huang, 2009). EEMD is considered more suited for multiple time scale analyses of nonlinear and non-stationary processes (Hawinkel et al., 2015; Li et al., 2018; Wen et al., 2017; Wu and Huang, 2009). EEMD was intended for long-term climate change analyses that mostly exhibit a nonlinear, non-stationary and complex process, with various time scales or periodic oscillations (Chen et al., 2017b; Franzke, 2014; Wei et al., 2018), and are spatially and temporally heterogeneous (de Jong et al., 2012; Huang et al., 2018; Ji et al., 2014; Myers-Smith et al., 2020; Pan et al., 2018). This method has been applied in many ecological assessments (Hawinkel et al., 2015; Liu et al., 2019; Liu et al., 2017a; Pan et al., 2018; Wei et al., 2018; Wen et al., 2017; Ye et al., 2019; Yin et al., 2017). Recently, based on EEMD analysis, interannual trends of the Normalized Difference Vegetation Index (NDVI) were quantified and the impacts on trends in climatic and environmental factors were analyzed (Ye et al., 2019). The spatial heterogeneity of vegetation dynamics in Southwest China has been revealed for different time scales (Liu et al., 2018). However, studies to estimate the length of periodic oscillations and the long-term trends in GPP have not been reported.

We know that the global annual average temperature increased 1.53 °C from the period 1885–1900 to the period 2006–2015 (Bereiter et al., 2015; Bongaarts, 2018; Chenguang et al., 2021). We also know that China is mainly dominated by the Eastern Asia monsoon climate and has experienced an increasing annual average temperature of 0.5–0.8 °C over the past 100 years (Ding et al., 2006; Qin et al., 2005). Between 1982 and 1999, climate change is believed to have prompted an increasing pace of growth of vegetation in terrestrial ecosystems globally by 6% (Nemani et al., 2003; Running et al., 2004). Multiple time scale analyses of the relationship between various climatic factors and vegetation dynamics in China, however, are lacking.

Therefore, this study used the EEMD and ridge regression methods to analyze the trends and impact factors of GPP in four climatic regions and at a national scale. The purpose was to: (1) explore long-term trends and the possible periodic oscillations in gross primary production time series; (2) analyze and diagnose the responses of the periodic oscillations to climate change; and (3) as the final objective, to understand vegetation changes in China and their underlying response mechanisms to climate change in the Eastern Asia monsoon climate.

2. Data and methods

2.1. GLOPEM-CEVSA model

The remote sensing-based ecosystem process model, GLOPEM-CEVSA, as shown in Figure S1, is based upon coupling of the Global Productivity Model (GLO-PEM) and the Vegetation, Atmosphere and Soil Carbon Exchange Model (CEVSA). This coupled model is based upon the concept of ecosystem simulation crossing multiple scales and the new generation of ecosystem models suggested by Cao et al. (2004). This coupled model has been tested at ecosystem flux observation sites (Wang et al., 2014; Wang et al., 2011a) and applied in ecological assessments and many other applications (Ouyang et al., 2021; Qian et al., 2022; Wang et al., 2022a). The model simulates the carbon cycle processes such as carbon turnover, carbon sequestration and carbon allocation, with the simulation results at the regional scale proved to be relatively accurate in comparison to other models (Sun et al., 2017). The model simulates photosynthetically active radiation (APAR) absorbed by vegetation using several data sources as input data, with details shown in Table 1, to output the GPP that visually represents changes in vegetation greenness (darker green represents higher productivity). The details on development of this model can be found in Wang et al. (2011a).

2.2. Data and processing

2.2.1. Meteorological data

An interpolated meteorological dataset was used as the model input, with a spatial resolution of 1 km and a temporal resolution of 8 days for the period from 1980 to 2018 in China (Wang and Ye, 2021). Interpolation software (ANUSPLIN) based on a smooth thin-plate spline algorithm (Hutchinson, 1995), developed by the Australian National University, was used in this study. The data were spatially interpolated based upon observations from 836 stations in China and 345 stations in surrounding countries, in which the effects of latitude, longitude and altitude on each climate variable were considered. The Digital Elevation Model (DEM) data used from the 90 m spatial resolution SRTM (Shuttle Radar Topography Mission) data (Farr et al., 2007) were resampled to 1 km spatial resolution as an interpolation co-variable. Thus, the errors in spatial interpolation that may be generated over the boundary area of the study region can be reduced. The interpolated data can explain 94% and 67% of spatial and seasonal variability in the weekly mean temperature and cumulative precipitation observations from ChinaFLUX and AsiaFLUX, which was considered being better than the corresponding data from other products (Wang et al., 2017a).

2.2.2. FPAR data

An 8-day 1 km Fraction of absorbed Photosynthetically Active Radiation (FPAR) dataset ($FPAR_{ANN)}$ from 1980 to 2018 (Zhang et al., In review) was used in this study. The $FPAR_{ANN}$ was derived from Global Inventory Modeling and Mapping Studies (GIMMS) Normalized Difference Vegetation Index, NDVI3g (Pinzon and Tucker, 2014) and the latest FPAR Collection-6 product, MCD15A2H C006, of Moderate Resolution Imaging Spectroradiometer (MODIS) (Myneni, 2015). The NDVI3g has data with a spatial resolution of 1/12° and a time step of half a month, but only covers the periods from 1981 to 2015. The MCD15A2H provides 500 m spatial resolution data products every 8-days from 2003 to the present. The two datasets were fused through a Back Propagation Artificial Neural Network (BP-ANN) algorithm and the $FPAR_{ANN}$ was generated for China's terrestrial ecosystems for the period 1981 to 2018. The $FPAR_{ANN}$ data provided a measure comparable to the flux towers-based GPP observations in term of seasonal changes and had more consistent results on trend, mean values and spatial variability than those derived from the MCD15A2H for the overlay period from 2003 to 2015 (Zhang et al., In review).

2.2.3. Vegetation, soil data and climatic regions

The vegetation classification data were derived from the Chinese national land cover database (ChinaCover2010) produced by the Institute of Remote Sensing and Digital Earth, Chinese Academy of Sciences (Zhang et al., 2014). The ChinaCover2010 with a spatial resolution of 250 m uses the IPCC classification scheme for terrestrial vegetation but reclassifies to the following 12 types: evergreen needle-leaf forest (ENF), evergreen broad-leaf forest (EBF), deciduous broad-leaf forest (DBF), deciduous needle-leaf forest (DNF), mixed forest (MF), savannas (SAV), woodland savannas (WSV), closed shrubland (CSH), open shrubland (OSH), grassland (GRS), cropland (CRP), and desert (DES). The vegetation data were resampled to a spatial resolution of 1 km, used as the model auxiliary data.

Soil texture data were used from a gridded Global Soil Dataset and were compiled through standardized data structure and data processing

Table 1
The input data for the GLOPEM-CEVSA model.

Input data	Periods	Temporal and Spatial resolution	Data sources and processing	References
Meteorological data	1980–2018	8-day, 1 km	Interpolated based upon observations from 1181 stations;	(Wang and Ye, 2021)
Fraction of absorbed Photosynthetically Active Radiation (FPAR) data	1980–2018	8-day, 1 km	Fused by Global Inventory Modeling and Mapping Studies (GIMMS) Normalized Difference Vegetation Index, NDVI3g and he latest FPAR Collection-6 product, MCD15A2H C006;	(Zhang et al., In review)
Vegetation classification data	2010	250 m	The Chinese national land cover database; Resampled to a spatial resolution of 1 km;	(Zhang et al., 2014)
Soil texture data	2014	30 rad seconds	The Global Soil Dataset; Resampled to a spatial resolution of 1 km and selected out area of China;	(Shangguan et al., 2014)
Digital Elevation Model (DEM) data	–	90 m	Resampled to 1 km spatial resolution;	(Farr et al., 2007)
Validation data	2003–2010/ 2004–2010	Daily scale; Sites scale	The Chinese Terrestrial Ecosystem Flux Research Network (ChinaFLUX); Interpolated to a temporal resolution of 8 days;	(Zhang et al., 2019a)

procedures from the Soil Map of the World and various regional and national soil databases (Shangguan et al., 2014). In this study, the data were resampled at a spatial resolution of 1 km from an original 30 rad seconds (about 900 m) using the method of nearest neighbor to match the meteorological data as input data for the model, including some soil information, such as soil particle-size distribution, organic carbon, and nutrients, and quality control information.

Climatic regions were defined by a climatic map of China (Editorial Committee, 2015). We classified the country into four climatic regions (i.e. temperate continental, temperate monsoonal, high-cold Tibetan Plateau and subtropical–tropical monsoonal) to investigate responses of the terrestrial GPP to climate changes in different climatic regions.

2.2.4. *Validation data*

The modeled GPPs were validated by comparing with the GPP observations from eddy covariance-based flux towers. The daily GPP observations are provided by ChinaFLUX, including four forest sites (CBS, QYZ, DHS, and XSBN), one shrubland (HBshrub), one wetland (HBwet), two grassland (NMG and DXGR), and one cropland site (YC)(Zhang et al., 2019a). The data were obtained by the continuous CO_2 flux measurement provided by individual researchers at each site and the quality of all data was controlled through the ChinaFLUX flux data processing system (Fu et al., 2006; Guan et al., 2006; Li et al., 2008; Liu et al., 2012; Wen et al., 2006; Yu et al., 2014; Yu et al., 2006). The weekly GPP estimates for the sites were extracted based on the latitude and longitude coordinates of the sites (Table 2).

The GPP estimates in this study were also evaluated by comparing with two other GPP datasets from the GOSIF and MODIS product (MYD17A2H). The GOSIF is from the global Orbiting Carbon Observatory-2 (OCO-2)-based Solar-induced chlorophyll fluorescence (SIF) data and has a spatial resolution of 0.05 latitude and longitude degrees and temporal resolution of 8-days over the period 2000–2020 (Li and Xiao, 2019; Lu et al., 2018; Qiu et al., 2020; Rossini et al., 2015; Wood et al., 2017). The MYD17A2H is based on the concept of radiation-use efficiency with a resolution of 500 m and a cumulative period of every 8-days from 2002 to 2017, and is widely applied to monitor vegetation growth (Qiu et al., 2020; Running et al., 1999; Running and Zhao, 2019; Turner et al., 2006; Zhao and Running, 2010).

2.3. *Analysis methods*

2.3.1. *EEMD*

The EEMD is an analysis method used to explore the intrinsic feature scale of the data by decomposing a time series based on the Hilbert-Huang transformation (Huang et al., 1998; Wu and Huang, 2009), naturally decomposing the signal into a series of signals with different characteristic intrinsic mode function (IMF) components and a trend component (Residual). Each IMF component with different signal frequencies represents the periodic characteristics of the original time series on a different time scale, while the residue reflects the long-term trend of the original sequence (Xiang et al., 2021; Zhang et al., 2020). In this study, it was accomplished through use of Matlab script (https://blog.csdn.net/imasupergril/article/details/96137828) and mainly included the following steps (Chen et al., 2020; Liu et al., 2018): First, a certain number, *np*, of Gaussian white noise, $\phi_j(t)$, is added to the original time series, $D(t)$, at time, t, to obtain a new time series with the noisy pseudo-signals, $D_j(t)$. Here, the number *np* was set as 100 as in previous studies (Jiao et al., 2020). It is generally recommended that the amplitude of the Gaussian white noise series be set to between 0.2 and 0.3 times the standard deviation of the original data (Chen et al., 2020). In this study, the standard deviation was set to be 0.2 (Chen et al., 2020; Liu et al., 2018).

$$D_j(t) = D(t) + \varphi_j(t) j = 1, 2, 3, \cdots .np \tag{1}$$

Second, the original time series, $Dj(t)$, was decomposed into the Intrinsic Mode Function (IMF) components, $IMF_i(t)$, and a trend component (residual), R_n, through the EMD method (Chen et al., 2017a; Huang et al., 1998).

Table 2
The ChinaFLUX sites and their descriptions, on which the GPP observations of 70 site-year data were applied to validate the corresponding estimation from the GLOPEM-CEVSA.

Site name	Latitude(°)	Longitude(°)	Altitude(m)	Vegetation type	Date year	Temporal scale
CBS	128.096	42.402	738	The temperate mixed forest	2003–2010	Daily scale
QYZ	115.063	26.747	100	The evergreen mixed forest	2003–2010	Daily scale
DHS	112.536	23.173	300	The evergreen needle-leaf forest	2003–2010	Daily scale
XSBN	101.266	21.950	750	The tropical rain forest	2003–2010	Daily scale
Hbshrub	101.331	37.665	3358	The alpine shrub-meadow	2003–2010	Daily scale
Hbwet	101.327	37.609	3357	The alpine swamp	2003–2010	Daily scale
NMG	116.675	43.545	1200	The temperate steppe	2004–2010	Daily scale
DXGR	91.066	30.497	4333	The alpine steppe-meadow	2004–2010	Daily scale
YC	116.640	36.958	28	The cropland	2003–2010	Daily scale

$$D_j(\mathrm{t}) = \sum_{i=1}^{np} IMF_I(t) + R_n(t) \quad (2)$$

Third, the first two steps were repeated by adding a new white noise of the same amplitude at each time, *t,* and then iterated *np* times.

Fourth, the *i*th IMF and final residual term are averaged:

$$IMF_i(t) = \frac{1}{np}\sum_{j=1}^{np} IMF_{ij}(t) and R_n = \frac{1}{np}\sum_{j=1}^{np} R_{nj}(t) \quad (3)$$

The periodic oscillation (T_i) of each IMF was calculated (Chen et al., 2017a; Liu et al., 2017a):

$$T_i = \frac{N}{P_i} \quad (4)$$

where N is the length of the IMF component and P_i is the number of peaks for the i-th IMF component.

The statistical significance of each IMF was estimated according to the distribution of energy (E_i) and the mean period (T_i) of the IMF relative to that of pure white noise. The significant level was set at 95% confidence level in this study.

$$\ln E_i + \ln T_i = 0 and E_i = \frac{1}{N}\sum_{t=1}^{N} [IMF_i(t)]^2 \quad (5)$$

The relative importance of the IMF components and residual term were assessed by the variance contribution percent (*VC*, %) as follows.

$$VC_i = \frac{Var(IMF_i)}{\sum_{i=1}^{n} Var(IMF_i) + Var(R_n)} \bullet 100\% \quad (6)$$

$$VC_r = \frac{Var(R_n)}{\sum_{i=1}^{n} Var(IMF_i) + Var(R_n)} \bullet 100\% \quad (7)$$

where $Var\ (IMF_i)$ is the variance of the i-th IMF_i and $Var(R_n)$ is the variance contribution of the residual term. The variance contribution quantifies the relative contribution of the components in the variance in the original time series. A larger value indicates a stronger fluctuation from the corresponding more important component (Chen et al., 2020; Jiao et al., 2020).

Contrasting the linear trend with ordinary least squares (OLS), the nonlinear accumulated trend can be estimated according to EEMD. The accumulated trend was estimated by the incremental value of the residual term at a given time t compared with the value at the initial time t_0.

$$T_{\mathrm{acc},t} = R_{n,t} - R_{n,t_0} \quad (8)$$

$$R_t = T_{\mathrm{acc},t} - T_{\mathrm{acc},t-1} \quad (9)$$

$$T_{eemd} = \frac{1}{\mathrm{N}}\sum_{t=1}^{N} R_t \quad (10)$$

where $R_{n,t}$ and $R_{n,t0}$ denotes the EEMD residual at time t and t_0, respectively. R_t is the change rate of the accumulative trend at time t. The total trend, T_{eemd}, of the residual term was quantified by the averaged R_{t} over the whole time period (Chen et al., 2020; Ji et al., 2014; Pan et al., 2018; Xue et al., 2019).

2.3.2. Ridge regression analysis

The ridge regression analysis (RRA) was applied to explore impacts of climate change on the vegetation growth measured through GPP in this study. The GPP or its residual component from EEMD analysis was designated the dependent variable and the climate factors, including the annual mean daily minimum (Tmin) and maximum (Tmax) temperature, annual total precipitation (Pre) and annual total solar shortwave radiation (SWRad), were independent variables. The RRA is considered to be an effective method to decrease multicollineartiy among independent variables and overcome the problem of overfitting (Hoerl and Kennard, 2012; Soner et al., 2019) and is more reasonable and scientific than the methods of Ordinary Least Squares-based regression analysis (Noora, 2020; O et al., 2021; Soner et al., 2019).

Generally, the OLS-based linear regression is formulated as follows:

$$Y = \beta \bullet X + \varepsilon \quad (11)$$

Here, Y is a vector representing n-dimensional observations, X is the corresponding $n \times p$ observation matrix containing p independent variables, β is a $p \times 1$-dimensional coefficient vector, and ε is an $n \times 1$-dimensional random vector. The β is estimated generally by OLS as the following:

$$\beta^{\wedge} = (X'^{*}X)^{-1} \cdot X' \cdot Y \quad (12)$$

According to Gauss–Markov theory, β is the best linearly unbiased estimate, and when there is a highly linearly unbiased estimate between the independent variables, although the least squares estimates are theoretically well characterized, the coefficients of the least squares method can be estimated but very unstable and lead to unreliable results (Jiao et al., 2017; Soner et al., 2019). Considering the effect of multicollinearity of the model on the estimation, ridge regression was considered to improve the OLS method, which is generally expressed as follows:

$$\beta_{RR}^{\wedge} = (X'^{*}X + k \cdot I)^{-1} \cdot X' \quad (13)$$

where k is the ridge parameter, usually $k \geq 0$. When $k = 0$, the ridge estimate is an OLS estimate and I is the unit matrix, where one set of ridge parameters is added to the diagonal of the X matrix to reduce the degree of pathology of the original least estimate and make the inversion relatively stable. In this study, ridge regression was applied with GPP as the dependent variable and temperature, precipitation and solar radiation as the independent variables. All variables are linearly detrended prior to ridge regression and the regression coefficients are used to quantify the influence of the independent variables on the dependent variable.

3. Result

3.1. Model validation

The modelled GPP was validated against the eddy covariance based GPP observations of 70 site-year in China and the linear regression results showed that the 8-day GPP model significantly correlated with the corresponding observations (Fig. 1). The multiple correlation coefficient (R^2) was 0.76 for all sites and varied from 0.55 (the temperate grassland at NMG) to 0.93 (the deciduous forest at CBS), which meant the GPP modelled has good performance to capture the seasonal changes in the observed GPP time series.

The GPP in this study was also evaluated by comparing it with two other GPP datasets obtained from the GOSIF and MODIS product (MYD17A2H) (Figure S2). In terms of R^2, the GPP in this study showed better performance than that of the MYD17A2H and was almost of the same capability as the GOSIF. The MYD17A2H can explain 67% of seasonal changes for all sites (the result varied from 18% to 83%), while GOSIF can explain 77% for all sites and varied from 35% (tropic forest) to 92% (temperate forest). The validation and evaluation illustrated that the GPP in this study showed the same data accuracy as other products, but with the advantage of both high spatial resolution and long time periods that other products do not have.

3.2. Changes in gross primary productivity for terrestrial ecosystems

3.2.1. Spatial patterns of GPP

The spatial pattern of the mean annual GPP decreased from southeast to northwest for the spatial heterogeneity of vegetation. The GPP average was 1131 gC $m^{-2}a^{-1}$ and varied from 500 to 3500 gC $m^{-2}a^{-1}$

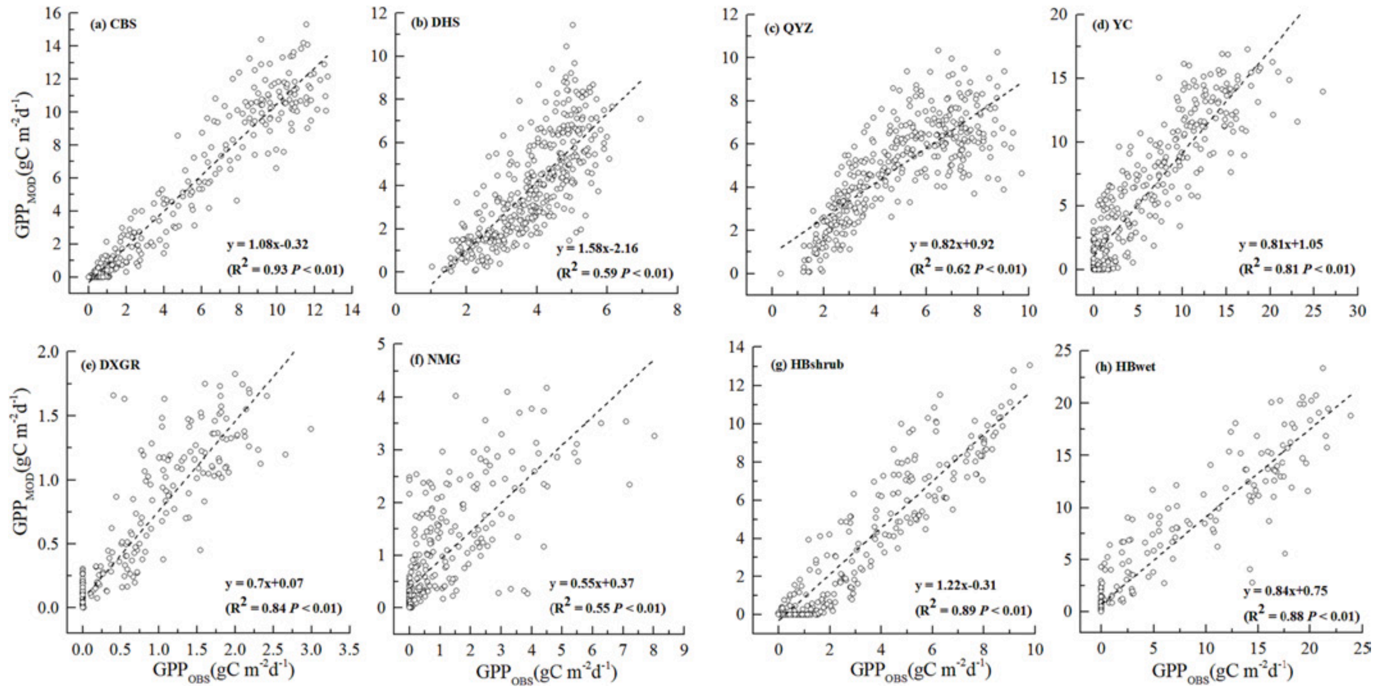

Fig. 1. The gross primary production (GPP) estimated by the GLOPEM-CEVSA models was validated against the eddy covariance observations of 70 site-year in China. These sites are Changbaishan temperate mixed forest (CBS, *a*), Dinghushan evergreen mixed forest (DHS, *b*), Qianyanzhou evergreen needleleaf forest (QYZ, *c*), Yucheng cropland (YC, *d*), Dangxiong alpine steppe-meadow (DXGR, *e*), Inner Mongolia temperate steppe (NMG, *f*), Haibei alpine shrub-meadow (HBshrub, *g*), and Haibei alpine swamp (HBwet, *h*). The goodness of fit was measured through linear regression and coefficient of determination (R^2).

with a confidence level of 95% from 1980 to 2018 over the terrestrial ecosystems of China (Fig. 2). Specifically, the GPP is more than 3500 gC $m^{-2}a^{-1}$ over forested areas in the southern China area; while the GPP is higher than 2000 gC $m^{-2}a^{-1}$ over areas where agriculture is the main vegetation type in central China. The grasslands and deserts have a lower GPP of<500 gC $m^{-2}a^{-1}$ over the Qinghai-Tibetan Plateau and the northwest of China. Compared to the average GPP for the first near 20 years of the period, the vegetation productivity increased in the most recent 20 year period for the whole country, especially in the south of China, with significantly more greening of vegetation (Fig. 2c).

3.2.2. *Interannual trends in GPP*

The interannual variability of vegetation measured by GPP could be decomposed to five time components in China for the period 1980 to 2018 based on the EEMD method (Fig. 3). As Table 3 shows, its residual component was significantly correlated to the original GPP time series (Spearman correlation coefficient, $r = 0.81$ and significant level, $p < 0.01$) and had the greatest variance contribution (77.10%). Among the four components of the GPP time series, the first component (IMF1) has the largest variance contribution at 11.25%.

For the four climate regions of China, the variance contributions of the residual components were still the greatest, which varied from 57.49% in the temperate monsoonal climate region to 84.59% in the subtropical–tropical monsoonal climate region. These results mean that the residual component plays a dominant role in the interannual variability of vegetation over the whole terrestrial ecosystem of China for the study period of 1980 to 2018.

The GPP showed an increasing trend quantified by its residual component from EEMD decomposition (Equation (9) and by the original GPP data-based OLS regression (Equation (11) on the pixel scale over

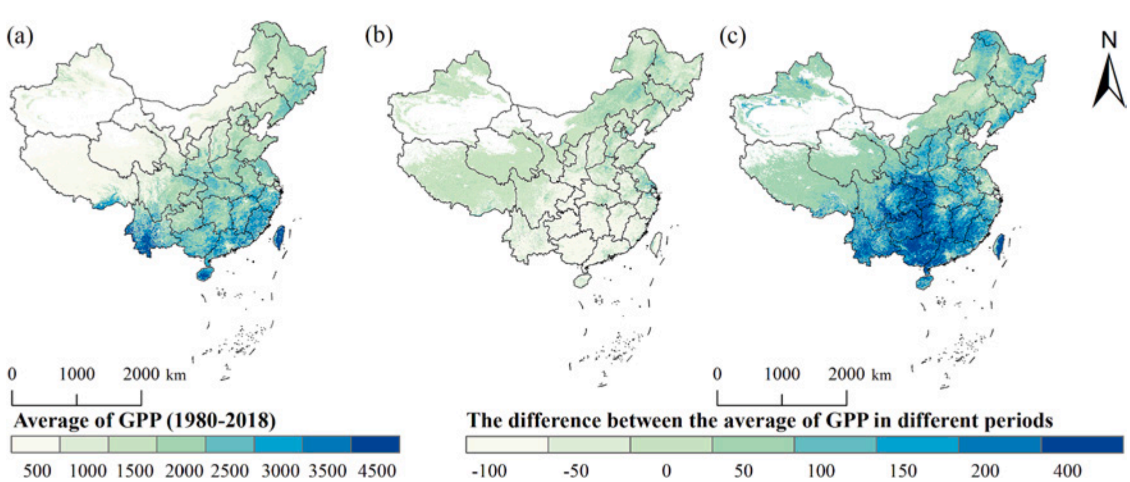

Fig. 2. The gross primary production (GPP), averaged, for the terrestrial ecosystems in China in the periods from (*a*) 1980 to 2018, (*b*) the difference in the average of GPP between 1980 and 2000 and 1980 to2018 and (*c*) the difference in the average of GPP between 2000 and 2018 and 1980 to2018.

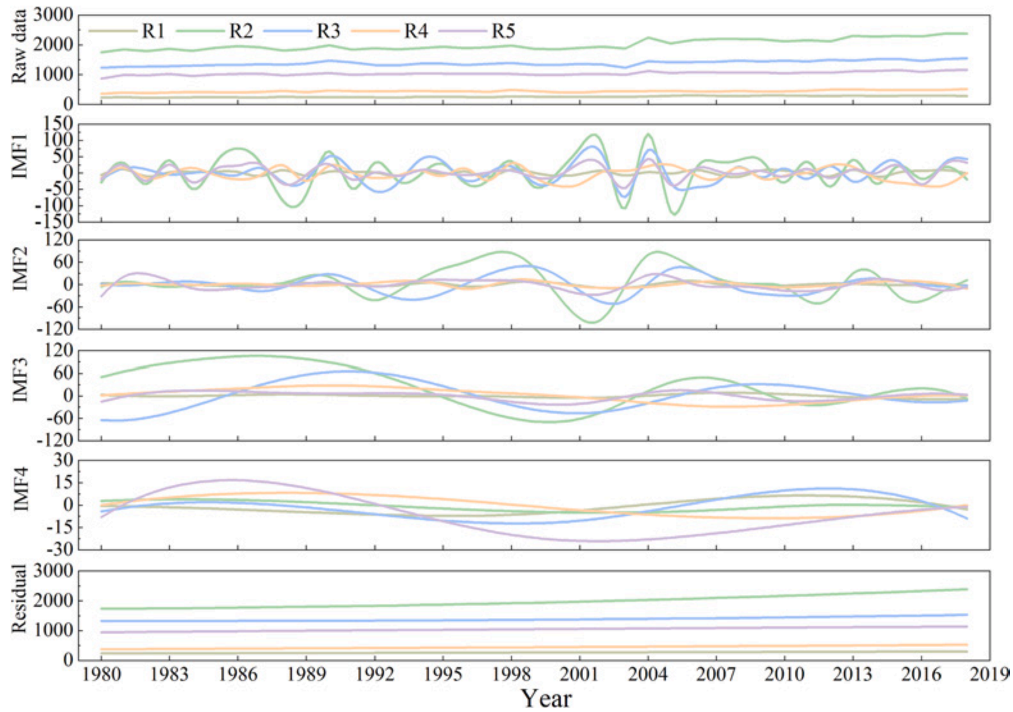

Fig. 3. The interannual variability of vegetation measured by GPP could be decomposed to five components through Ensemble Empirical Mode Decomposition (EEMD) for the entire country and the four climatic regions in China from 1980 to 2018 (R1 - High-cold Tibetan Plateau climate region; R2 - Subtropical-tropical monsoonal climate region; R3 - temperate monsoonal climate region; R4 - temperate continental climate region; R5 - Entire country).

Table 3
The results of Ensemble Empirical Mode Decomposition (EEMD) analysis for the gross primary production for the entire country and the four climatic regions in China in the period from 1980 to 2018.

		IMF1	IMF2	IMF3	IMF4	Residual
Entire country	Quasi-period	2.79	5.57	9.75	19.5	
	Variance contribution (%)	11.25	4.67	2.84	4.15	77.10
	Spearman	0.4623**	0.0808	0.0089	−0.1927	0.8093**
High-cold Tibetan Plateau	Quasi-period	3.00	6.50	13.00	39.00	
	Variance contribution (%)	10.17	3.74	4.32	4.03	77.75
	Spearman	0.3719*	0.1670	−0.0628	0.6164**	0.8721**
Subtropical-tropical monsoonal	Quasi-period	2.79	6.50	13.00	19.50	
	Variance contribution (%)	5.81	3.57	6.01	0.02	84.59
	Spearman	0.3897*	0.1065	−0.2917	−0.2947	0.8504**
Temperate monsoonal	Quasi-period	3.25	7.80	19.50	19.50	
	Variance contribution (%)	15.01	7.98	18.82	0.70	57.49
	Spearman	0.3512*	0.1308	0.3381*	0.3937**	0.8012**
Temperate continental	Quasi-period	3.90	6.50	19.50	39.00	
	Variance contribution (%)	13.57	1.34	11.34	1.37	72.38
	Spearman	0.3868*	0.1856	−0.1931	−0.2966	0.6915**

Note: * significant level, $p \leq 0.05$, and ** $p \leq 0.01$.

the terrestrial ecosystems in China for the period 1980 to 2018 (Fig. 4). The GPP increased by a rate ranging from 57.4 Mt C $m^{-2}a^{-1}$ (OLS) to 59.8 Mt C $m^{-2}a^{-1}$ (EEMD) and the area with a significant ($p < 0.05$) increasing trend accounts for 92% of the whole terrestrial ecosystem of China. The high-cold Tibetan Plateau climate region has the slowest increasing rate in GPP among the four major climate regions and accounts for 7.5% of the GPP increment in China (Fig. 5). The subtropical–tropical monsoonal climate region has the largest GPP growth rate, 8.4 times (EEMD) and 7.7 times (OLS) the rate of change of the high-cold Tibetan Plateau climate region, contributing 61.3% (EEMD) and 62.7% (OLS) for 7.5% of the GPP increment in China. There is little difference between the EEMD and OLS-based GPP trends in the temperate monsoonal climate region, with the same incremental contribution to the GPP change in China (18%). The incremental contribution was concentrated in the northeastern and western parts of climate regions. The difference between non-linear and linear GPP trends is greatest in the temperate continental climate region, where the non-linear rate of change is 6.1 Mt C $m^{-2}a^{-1}$ faster than the linear, and its contribution to GPP change in China can reach 12.9% and 10.5%, respectively. Overall, there is spatial heterogeneity in the GPP of terrestrial ecosystems in China, but it has always maintained a long-term stable upward trend in change.

Compared to the previous 20 years period (1980 to 2000), a significant upward trend of the GPP was found in the most recent 20 years from 2000 to 2018 (Fig. 5). In 2000 to 2018, the upward trends were 83.5 Mt C a^{-1} and 103.5 Mt C a^{-1} respectively based on the EEMD and OLS methods in China, which were 231% and 340% of the previous 20 year period trends, that is, 36.1 Mt C a^{-1} and 30.4 Mt C a^{-1}.

Vegetation growth acceleration with spatial heterogeneity varied across climatic regions. Compared to other climatic regions of China, the high-cold Tibetan Plateau climate region had the lowest contribution to the whole country's GPP trend, that is, only 1/20th of the non-linear

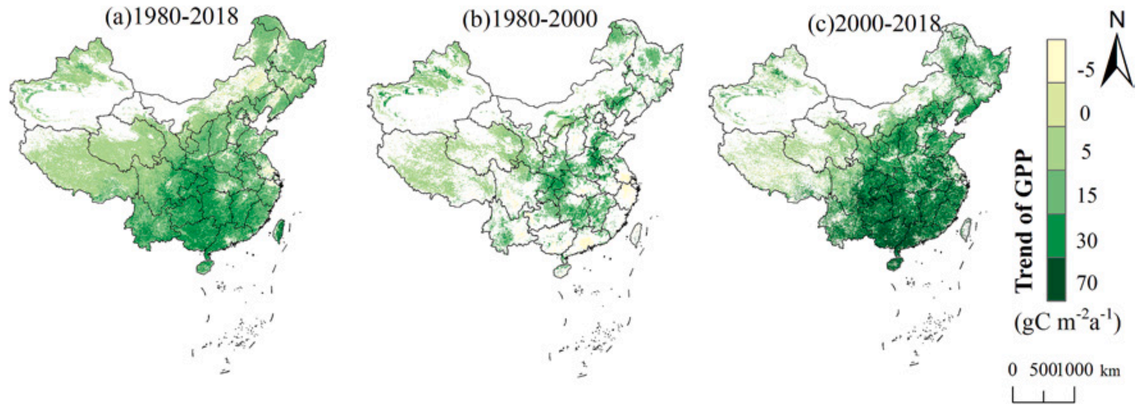

Fig. 4. The inter-annual trends in the GPP time series of Chinese terrestrial ecosystems in the three periods from 1980 to 2018 (*a*), the first (*b*) and recent (c) near 20 years of the period. (the colored area is statistically significant at $p \leq 0.05$).

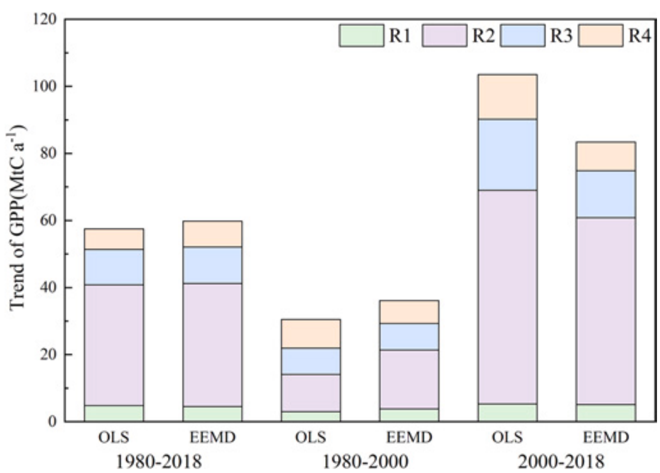

Fig. 5. Comparison of the trends for the EEMD-based nonlinear and OLS-based linear models of GPP for the four climatic regions in China. (R1 - High-cold Tibetan Plateau climate region; R2 - Subtropical-tropical monsoonal climate region; R3 - temperate monsoonal climate region; R4 - temperate continental climate region).

change and 6.1% of the linear change in the most recent 20 years and the contribution decreased 4.5% from that in the previous 20 years. The subtropical–tropical monsoonal climate region contributed to the major upward trending in GPP with a contribution of 61.5% (EEMD) and 66.7% (OLS) in the most recent 20 years, which is 1.7 and 1.4 times more than the corresponding values before 2000. The temperate monsoonal climate region contributed 25.5% and 20.8% of the non-linear and linear change of the GPP in 1980–2000, decreasing by more than 4% for 2000–2018. The temperate continental climate region showed an increase in the contribution to the nonlinear and linear trends of GPP by 15.4% and 8.4% after 2000, respectively. Compared to the previous 20 years, the trend of GPP increased in the range of 2.33–52.58 Mt C m^{-2}a^{-1} (EEMD) and 1.31–38.08 Mt C m^{-2}a^{-1} (OLS) across the four climate regions in the most recent 20 years, with a substantial increase of contribution for the subtropical–tropical monsoonal climate region.

3.2.3. Periodic oscillation in GPP

Vegetation growth was found to have a periodic oscillation, measured by the EEMD method, for the GPP time series (Fig. 3 and Table 3). The first component (IMF1) of GPP was significantly correlative with the original time series ($r = 0.47$, $p < 0.01$) and oscillated in a 2.79-years cycle over the whole terrestrial ecosystem of China. Meanwhile, the dominant component and its periodic years varied across climatic regions. The high-cold Tibetan Plateau climate region showed almost the same as the whole country, while the third component (IMF3) was dominant in the interannual variability of GPP and had a periodic oscillation of about 13 years in the subtropical–tropical monsoonal climate region. In the temperate monsoonal and temperate continental climate regions, the preponderant influence of the contribution can be attributed to the first and third fluctuating components (IMF1 and IMF3) with a periodic oscillation of about 3.25-years and 19.5-years, 3.9-years and 19.5-years, respectively. These results demonstrated that the short-term (approximately 3 years) and long-term (approximately 20 years) oscillation control the inter-annual and -decadal variability of the vegetation growth measured by the GPP over Chinese terrestrial ecosystems.

3.3. Climate change and its impacts on GPP

3.3.1. Periodic oscillation in climate change

The interannual variability of precipitation was best characterized as periodic oscillation with an increasing trend not evident in the research region (Table S1 and Figure S3). The first component (IMF1) played the major contribution with a variance contribution of more than 53% with a periodic oscillation of 2.6 to 3.25-years in the interannual variability of precipitation over most regions except Subtropical-tropical monsoonal climate region in China. As an exception, in the subtropical–tropical monsoonal climate region, the first, third and fourth components had almost the same variance contribution of between 22.42 and 28.13 and is characterized as periodic oscillation from the short-term of 3.25-year to the long-term of 19.50-year in its precipitation variability. Therefore, the precipitation periodically oscillated by a short-term cycle of about 3-years over most of China.

The air temperature, on the contrary, interannually varied with a long-term warming trend, but its periodic oscillation was not evident and varied depending on the region of China. The residual component contributed the most to explaining variance with over 60% in the interannual variability of the annual mean daily minimum, maximum and mean temperatures (Table S2-4), which means the long-term trends dominated the interannual variability of air temperature.

Both a long-term trend and periodic oscillation were found in the interannual variability of solar radiation over the whole country (Figure S3 and Table S5). The solar radiation was dominated by its residual component with the highest variance contribution of 63%, along with the first component having the second highest contribution of 27% on the national scale. The first component, however, played a major contribution and had about a 3-years quasi-periodic oscillation over the subtropical–tropical monsoonal climate region, the temperate monsoonal and the temperate continental climate regions, except the high-cold Tibetan Plateau climate region where there was a long-term increasing trend with the greatest variance contribution (50.61%).

Table 4
Ridge regression analysis was applied to gross primary production (GPP) and the its residual component to explore the impacts from climate change for the entire country and the four climatic regions in China for the period from 1980 to 2018. The climate change factors considered here were the annual total precipitation (Pre), annual mean daily maximum temperature (Tmax), annual mean daily minimum temperature (Tmin) and annual total shortwave solar radiation (SWRad).

Data	Climatic region	Standardized regression coefficients				R^2
		B_{Pre}	B_{Tmax}	B_{Tmin}	B_{SWRad}	
Original GPP	Entire country	−0.06	0.19	0.22	−0.11	0.55
	High-cold Tibetan Plateau	0.06	0.23	0.29	−0.01	0.78
	Subtropical-tropical monsoonal	−0.07	0.23	0.25	−0.01	0.63
	Temperate monsoonal	0.02	0.16	0.21	−0.12	0.45
	Temperate continental	0.21	0.11	0.17	−0.08	0.48
EEMD-based residual of GPP	Entire country	−0.06	0.21	0.24	−0.21	0.84
	High-cold Tibetan Plateau	0.03	0.21	0.28	−0.10	0.75
	Subtropical-tropical monsoonal	−0.06	0.23	0.27	−0.08	0.72
	Temperate monsoonal	−0.02	0.15	0.19	−0.19	0.52
	Temperate continental	0.02	0.17	0.24	−0.06	0.50

3.3.2. Impacts of climate change on vegetation growth

The variability in GPP and its EEMD-based residual component can be well explained by climate change in China. Climate change can explain variability of 55% and 84% in the GPP and its residual component on the national scale according to the multiple correlation coefficient (R^2) of the ridge regression analysis (Table 4). Among the four climate regions, the vegetation growth measured by GPP was more impacted by climate change with the higher R^2 of 0.78 and 0.63 in the high-cold Tibetan Plateau climate region and Subtropical-tropical monsoonal region. Meanwhile, the R^2 was 0.45 and 0.48 in temperate monsoonal and continental regions, respectively, which was lower than the previous two regions. For the residual component of GPP, the difference was almost the same among the regions, however, it should be noted that the R^2 was higher than that for the GPP itself, which means the long-term trend measured by the residual components were more impacted by climate change than the GPP itself.

The interannual variability of the vegetation growth measured by GPP was dominantly impacted by the Tmin among the considered climatic variables, according to the ridge regression analysis (Table 4). By comparing the regression coefficients, the impacts of climate change could be quantified by the inter-annual variability and long-term trend of GPP. As shown in Table 4, the variability in GPP was positively impacted by a warming climate with the regression coefficients of 0.19 ~ 0.24 for the Tmin and Tmax, while they were −0.06 and −0.11 for the Pre and SWRad, respectively, owing to their insignificant (Slope = -0.18, R^2 = 0.003) and significant (Slope = -1.88, R^2 = 0.53) decreasing trends. Furthermore, the regression coefficients of Tmin were 15.79% and 14.29% higher than those of Tmax, which means Tmin exerted an overwhelming effect on the variability and long-term trend of the GPP in this study.

The change of Tmin has the greatest influence on both interannual variability and long-term trends in GPP in each climate region, except the temperate continental climate region. In the temperate continental climate region, the change in precipitation had maximum effect on the inter-annual variability of GPP with a regression coefficient of 0.21, but it's still Tmin playing an overwhelming role on the long-term trend of GPP with a coefficient of 0.24. The effects of Tmin were 26.09%, 8.70%, 31.25% and 54.55% higher than that of Tmax on the long-term trends of the GPP in the four climate regions of the high-cold Tibetan Plateau climate region, the subtropical–tropical monsoonal climate region, the temperate monsoonal climate region and the temperate continental climate region, respectively (Figs. 6-7).

4. Discussion

4.1. Uncertainty in the model

The modelled GPP was evaluated and compared against the eddy covariance-based observations in this study and the results showed the modeled GPP was better than the MODIS-based GPP (MYD17A2H) and comparable with GOSIF-based GPP (GOSIF) estimates (Fig. 1 and Figure S2). The sources of uncertainty for modeled results are mainly from the model structure, model parameters and input data (Li et al., 2016; Li et al., 2022; Yan et al., 2019). The study estimated GPP based on GLOPEM-CEVSA at the spatial resolution of 1 km^2 from 1980 to 2018, using interpolated meteorological data with great accuracy and the FPAR data with a long time series of about 40 years fused for two datasets with different time series (Wang and Ye, 2021; Zhang et al., In review). The average annual vegetation productivity measured by GPP in China was 8.02 Pg C a^{-1}, which was within the range of modelled results from previous studies (Table 5). Compared with other models, this result proves more accurate for fine spatial resolution and long time series.

On the other side, uncertainties exist in flux tower data due to eddy-covariance-based data observations and processes, and the scale mismatch between remote sensing-based GPP and eddy covariance-based observations (Hagen et al., 2006). However, these on-the-ground-based observations are only data to evaluate the modelled data, which are representative for typical regional climate and ecosystem.

The exploration of reducing uncertainty in model simulations always is a challenge to improve the accuracy of GPP assessments for terrestrial ecosystems. The SIF has been found to be more correlative with plant photosynthesis and the SIF-based GPP was considered to be more accurate (Feng et al., 2019; Liu et al., 2017b; Qiu et al., 2020). Therefore, the SIF-based data assimilation and parameterization should be further developed to further improve the accuracy of GPP estimation. Meanwhile, more eddy covariance-based GPP observations are necessary and essential as the benchmark for model assimilation and parameterization.

4.2. Periodic oscillation in GPP interannual variability

Vegetation growth is affected by cyclical climate changes. The variability of vegetation growth measured by GPP had a periodic oscillation of about 2.79 years and varied across the different climate regions, which is likely driven by the East Asia monsoon climate (Li, 2021; Li et al., 2015). The EEMD analysis was conducted on the new East Asian Monsoon Index (EAMI) and the four fluctuating components (IMF1-4) showed the oscillating periods of 2.6, 5.57, 13 and 19.5 years with variance contributions of 70.85%, 21.83%, 1.36% and 0.28%, respectively (Figure S4). Therefore, the East Asian monsoon oscillates by a quasi-period of about 3 years, which was within that previously reported by Zhou et al (2008)of a 3–7 year cycle.

The East Asian monsoon significantly influences summer precipitation in eastern China, thereby directly affecting vegetation productivity (He et al., 2019; Yu et al., 2014; Zhang et al., 2019b; Zhang, 2020). As the Qinghai-Tibetan Plateau climate region is inland in western China, the fluctuation variability in vegetation was mainly dominated by short 3-year periods with less influence from the East Asian monsoon. In the other three eastern climatic regions located in eastern China, however, the periodic oscillations of the GPP time series influenced by the monsoon precipitation showed a short cycle of 3 years and a significant long cycle of 13 or 20 years. The East Asian monsoon oscillations would

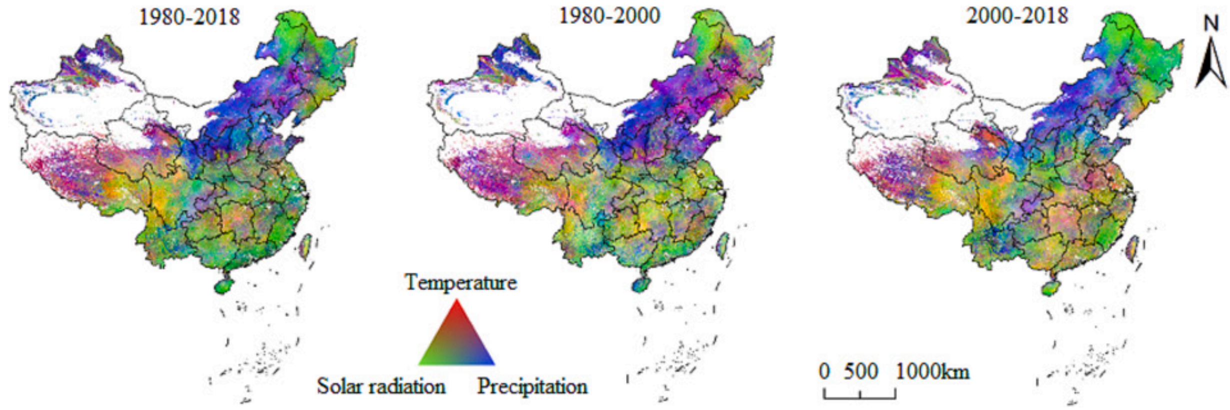

Fig. 6. Impact of climate factors on GPP in terrestrial ecosystems in China from 1980 to 2018 and the previous and most recent 20 years.

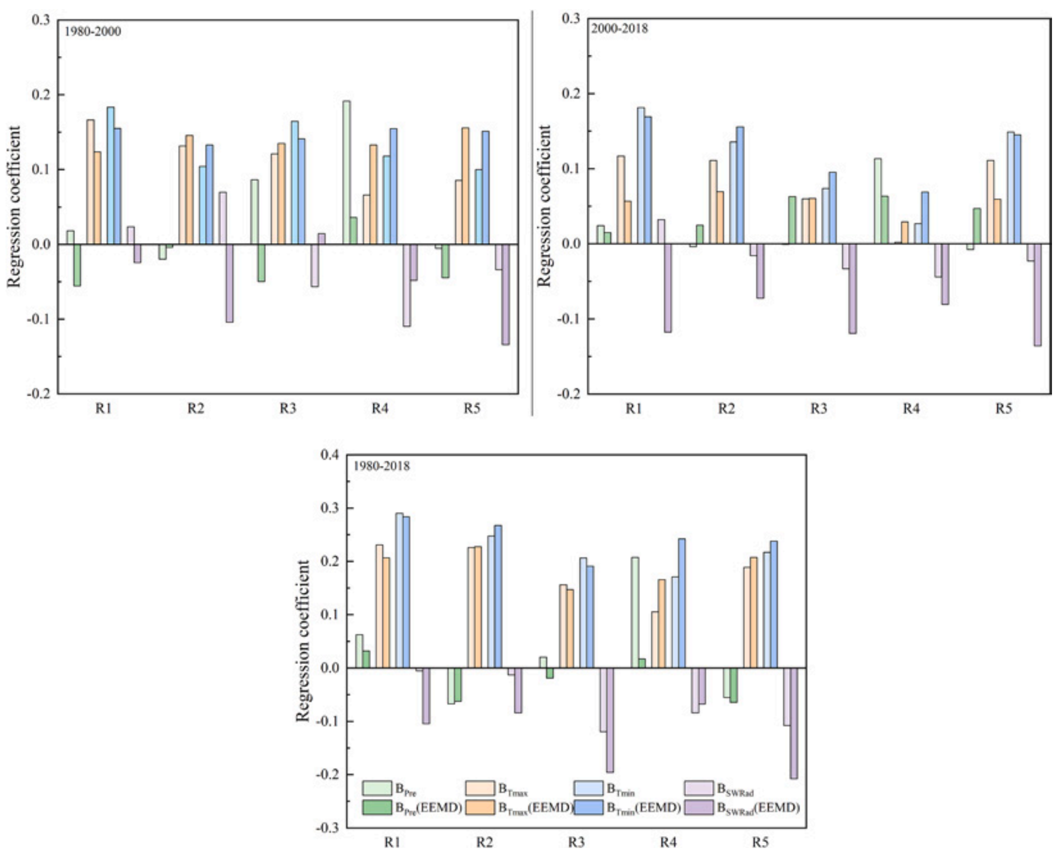

Fig. 7. The ridge regression analysis-based regression coefficient for the gross primary production (GPP) and its residual component with the climate variables for the entire country and the four climatic regions in China during the period from 1980 to 2018 and the most recent 20 years. (R1 - High-cold Tibetan Plateau climate region; R2 - Subtropical-tropical monsoonal climate region; R3 - temperate monsoonal climate region; R4 - temperate continental climate region; R5 - Entire country).

result in a quasi-oscillation in vegetation change by influencing climate change.

Vegetation oscillations are merely a result of periodic environmental variability, or rather they are driven by endogenous factors (Tzuk et al., 2019). The oscillations are a manifestation or aggregate of a complex relationship between human activity and cyclical climate change, probably linked to the El Niño-Southern Oscillation against the background of long-term climatic change (Barbosa et al., 2020; Xu et al., 2019). Increasing our knowledge about how vegetation responds to climate variability is of high importance for managing ecosystems in a future of global climate change.

4.3. Impacts of climate change on GPP

Vegetation responses to climate change are very complex and greatly vary in space and time (Ahlstrom et al., 2015; Nemani et al., 2003). This study found that GPP increased with a long-term significant upward trend with great spatial heterogeneity over the terrestrial ecosystems of China. Climate change, especially changes in daily minimum air temperature, exerts an overwhelming effect on the inter-annual variability and long-term trend of GPP. The correlation between temperature and vegetation growth was found to be high in China (Cao et al., 2022; Chuai et al., 2020; Deng et al., 2022; Liu et al., 2022). Climate warming prolongs the growing season, which greatly contributes to the greenness and productivity of vegetation (Keenan and Riley, 2018). The minimum

Table 5
Estimations of GPP in different terrestrial ecosystem models over China.

Model and method name	Study period	Spatial resolution	Average annual gross primary productivity/ (Pg C a^{-1})	References
LUE (Light use efficiency model)	1990	8 km	12.26	(Chen et al., 2001)
TL-LUE (Two-leaf light use efficiency model)	2003–2017	500 m, 1 km, 500 m	6.60, 7.46, 6.39	(Hou et al., 2020)
TL-LUE, MTE (Model tree ensemble)	2007–2011	0.5°	7.17, 7.47	(Zan et al., 2018)
TL-LUE	1981–2012	0.0727°	7.64	(Zhou et al., 2020)
EC-LUE (Eddy Covariance-Light Use Efficiency)	2000–2009	10 km	6.04 (5.63–6.39)	(Li et al., 2013)
EC-LUE	2000–2003	0.5°×0.6°	5.38	(Yuan et al., 2010)
EC-LUE	2008–2009	1 km	5.55	(Cai et al., 2014)
CASA (Carnegie-Ames-Stanford approach)	1982–1999	0.1°	2.66–3.16	(Piao et al., 2005)
CASA	1989–1993	8 km	6.24	(Zhu et al., 2007)
CEVSA (Carbon Exchange between Vegetation, Soil and Atmosphere)	1981–1998	0.5°	6.18	(Tao et al., 2003)
GEOPRO (Geo-Process model based eco-system photosynthesis theory), CEVSA, GLOPEM (Global Production Efficiency Model), GEOLUE, CASA	2000, 1980–2000, 1981–2000, 2000–2004, 1982–2003	4 km, 10 km, 8 km, 8 km, 8 km	4.84, 6.26–7.36, 5.52–6.62, 5.68, 5.14–5.92	(Gao and Liu, 2008)
CEVSA-RS	2000–2017	0.1°	7.21, 6.83	(Wang et al., 2021)
MOD17	2000–2010	1 km	5.09	(Running et al., 2004)
MOD17	2000–2014	1 km	5.53	(Zhao et al., 2004)
BEPS (Boreal Ecosystem Productivity Simulator)	2001	1 km	4.42	(Feng et al., 2007)
BEPS	2000–2010	500 m	5.26–5.68	(Liu, 2013)
Vegetation Photosynthesis Model-Evaporative Fraction	2003–2009	5 km	5.48	(Qiu, 2015)
VPM (Vegetation Photosynthesis Model)	2000–2016	500 m	6.74	(Ma et al., 2019)
VPM	2006–2008	0.5°	5.00	(Piao et al., 2014)
MTE, Geographical assessment schemes	2001–2011, 2001–2010	0.5°, 10 km	6.06, 7.78	(Wang et al., 2015a)
MTE	1982–2015	0.1°	6.62	(Yao et al., 2018)
MTE	1982–2010	0.5°	6.35	(Jung et al., 2011)
TBMs(Terrestrial Biosphere Model), MTE	1981–2010	0.5°	7.4, 7	(Jia et al., 2020)
MTE, MODIS17, CLM4-CN (Community Land Model version 4 with Carbon Nitrogen interactions)	2000–2004	0.5°	6.9, 5.9, 13.7	(Wang et al., 2015b)
MODIS, TEC (Terrestrial Ecosystem Carbon flux model), BESS (Breathing Earth System Simulator)	2000–2015	5 km, 0.5°, 0.5°	5.97, 7.03,6.42	(Wang et al., 2021; Yan et al., 2019)
Multiple regression	2001–2010	1 km	7.51	(Zhu et al., 2014)
SVR (Support Vector Regression)	2000–2015	0.25°	7.81	(Ichii et al., 2017)
DLM (Dynamic land model), FLUXCOM GPP (Eddy-covariance measurements)	1980–2013	0.5°	5.56, 6.53	(Du et al., 2020)
CABLE (CSIRO Atmosphere and Biosphere Land Exchange), CLM4, LPJ (Lund-Potsdam-Jena Dynamic Global Vegetation Model), ORCHIDEE (Organizing Carbon and Hydrology In Dynamic EcosystEms), VEGAS (Vegetation Global Atmosphere Soil)	1982–2010	0.5°	7.97 (6.14–9.76)	(Li et al., 2016)
GOSIF-GPP (Global OCO-2-based solar-induced chlorophyll fluorescence dataset), DTEC-GPP (Diffuse-fraction-based two-leaf light	2001–2018	5 km	7.23, 6.93	(Zhang et al., 2021)

(continued on next page)

Table 5 (*continued*)

Model and method name	Study period	Spatial resolution	Average annual gross primary productivity/ (Pg C a^{-1})	References
use efficiency model)				
GLOPEM-CEVSA	1980–2018	1 km	8.02	The study

daily temperature has an overwhelming effect on growth and development processes, such as the end of the vegetation dormancy period, the growth of shoots and the unfolding of leaves (Horvath et al., 2003; Körner, 2015). On the one hand, the excessively low night-time temperature harms the cellular structure of plants and slows down or delays the developmental processes of vegetation (Shen et al., 2016; Vitasse et al., 2014). On the other hand, it also affects the water uptake of vegetation roots through soil freezing, limiting the supply of soil water to vegetation during the period of thawing in spring and delaying the time of the thaw (Wan et al., 2012; Wang et al., 2022b; Yang et al., 2013).

Warming substantially promotes vegetation growth by alleviating temperature constraints, lengthening growing season, and enhancing photosynthesis (Bi et al., 2013; Lucht et al., 2002; Myneni et al., 1997; Wang et al., 2017b). Warming daily minimum temperature slows the risk of frost to vegetation and accelerates the melting of snow and ice in the high-cold Tibetan Plateau climate region, resulting in sufficient soil moisture for vegetation after a dry winter and early spring (Cao et al., 2022; Keenan and Riley, 2018; Liu et al., 2022; Shen et al., 2016; Wang et al., 2022b). A warming, humid climate effectively enhances the photosynthesis of vegetation and prolongs the growing season, promoting the growth of vegetation in the temperate monsoonal climate region (Cao et al., 2022; Jiao et al., 2019; Keenan and Riley, 2018; Sun et al., 2021). But the positive effect of warming on vegetation growth has weakened in recent years (Piao et al., 2017; Piao et al., 2014). Warmer summers could decrease plant productivity in extra-tropics (Angert et al., 2005).

Increases in precipitation can effectively mitigate the decline in plant transpiration and photosynthesis caused by drought stress in water-deficient regions, enhancing soil moisture and promoting vegetation growth (Saatchi et al., 2013; Zhou et al., 2014). The growth of vegetation is sensitive to precipitation in the temperate continental climate region, as shown in Table 4, which is consistent with previous results, that precipitation is the main factor for vegetation growth in arid and semi-arid regions of northern China (Cao et al., 2022; Chuai et al., 2020; Shi et al., 2021; Zhao et al., 2022). In water-limited ecosystems, changes in precipitation dominates inter-annual trends in vegetation and even result in desertification (D'Odorico et al., 2013; Zhou and Jia, 2016). In some local places of semi-arid regions of Northern China, desertification is still serious due to drought (Kang et al., 2018; Wang et al., 2011b).

The air temperature as an important climate factor dominates the trend of GPP in China. Warming accounted for at least 42% of the increasing trend in GPP in this study, while an insignificantly decreasing trend of precipitation had a weakly negative correlation with vegetation productivity, contributing no more than 0.5% to productivity. Consequently, the influence of temperature on vegetation productivity was much higher than the influence of precipitation. Meanwhile, a threshold exists for the contribution of precipitation (Felton et al., 2021; Wang et al., 2023), especially in forest vegetation types in the relatively humid climate of southern China (Xu et al., 2020). It is essential for relatively moist vegetation to receive a moderate amount of precipitation (Brandt et al., 2018). The negative correlation between precipitation and vegetation productivity in the subtropical–tropical monsoonal climate region, as shown in Table 4, may be explained by the occurrence of such conditions as flooding because of an excessive amount of precipitation in summer, aggravating the anaerobic environment in the roots, reducing soil nutrients and restraining vegetation growth (Fu et al., 2016; Schuur et al., 2001; Yang et al., 2015).

The contribution of solar radiation changes to the increasing trend of GPP is relatively weak. The annual total shortwave solar radiation across the entire country and climate regions in this study showed a significant decreasing trend and a negative correlation with vegetation growth, accounting for only about 10% of the vegetation productivity trend in China. Generally, increasing solar radiation can effectively promote vegetation growth in tropical forests by improving plant photosynthesis and enhancing the rate of dry matter fixation by vegetation (Nemani et al., 2003). The overwhelmingly dominant contribution of temperature change to the trends of vegetation productivity in this study was much greater than the effect of solar radiation. In addition, the synergistic effects of temperature, precipitation and solar radiation on vegetation productivity are complex and may be interactivity or extinction, while also exhibiting significant geographical differences (Xu et al., 2020), which also explains the differences in the correlation between climatic factors and vegetation growth among the different climatic regions in this study. Given the complex processes in the climate system itself and the interaction between biosphere and atmosphere (Feng et al., 2019; Li, 2021; Li et al., 2015), further simulation and analysis are essential to understand responses of terrestrial ecosystems to climate change in future studies.

5. Conclusion

Gross Primary Productivity (GPP), as a quantified photosynthesis indicator, is widely applied in ecosystem research. In this study, the GPP was estimated at 1 km^2 spatial resolution for the terrestrial ecosystems of China for nearly 40 years from 1980 to 2018. The interannual variability in the GPP time series was decomposed through Ensemble Empirical Modal Decomposition (EEMD) and its underlying mechanism was quantified in terms of climate change. The variability of GPP over the nearly 40 years was driven by a long-term increasing trend accompanying a periodic oscillation of nearly 3 years. And its increasing rate in the last 20 years is more than twice of that in the previous 20 years, and warming evidenced by increased daily minimum temperatures may be a vital contributor to ecosystem changes. This study offers new insight by decomposing vegetation measurement time series to diagnose intrinsic mechanisms in ecosystem response to climate change. These results can improve our understanding and prediction in ecosystems and productivity changes and are essential for policy-making to mitigate and adapt to climate change.

Funding

The Second Tibetan Plateau Scientific Expedition and Research (STEP) program (Grant No. 2019QZKK0302-02), the National Natural Science Foundation of China (31971507), the CAS-Qinghai Province Joint program on Three-River Headwaters National Park (LHZX-2020–07).

CRediT authorship contribution statement

Chan Zuo: Methodology, Software, Writing – original draft, Writing – review & editing. **Junbang Wang:** Conceptualization, Methodology, Writing – original draft, Writing – review & editing, Funding acquisition. **Xiujuan Zhang:** Supervision, Writing – review & editing. **Alan E. Watson:** Writing – review & editing.

Declaration of Competing Interest

The authors declare that they have no known competing financial interests or personal relationships that could have appeared to influence the work reported in this paper.

Data availability

Data will be made available on request.

Appendix A. Supplementary data

Supplementary data to this article can be found online at https://doi.org/10.1016/j.ecolind.2023.110704.

References

Ahlstrom, A., et al., 2015. The dominant role of semi-arid ecosystems in the trend and variability of the land CO_2 sink. Science 348 (6237), 895–899.

Anav, A., et al., 2015. Spatiotemporal patterns of terrestrial gross primary production: A review. Rev. Geophys. 53 (3).

Angert, A., et al., 2005. Drier summers cancel out the CO_2 uptake enhancement induced by warmer springs. PNAS 102 (31), 10823–10827.

Ballantyne, A., et al., 2017. Accelerating net terrestrial carbon uptake during the warming hiatus due to reduced respiration. Nat. Clim. Chang. 7 (2).

Barbosa, J.M., Pascual-Rico, R., Martinez, S.E., Sanchez-Zapata, J.A., 2020. Ungulates Attenuate the Response of Mediterranean Mountain Vegetation to Climate Oscillations. Ecosystems 23 (5), 957–972.

Beer, C., et al., 2010. Terrestrial gross carbon dioxide uptake: global distribution and covariation with climate. Science 329 (5993).

Bereiter, B., et al., 2015. Revision of the EPICA Dome C CO_2 record from 800 to 600kyr before present. Global Warming. Focus.

Bi, J., Xu, L., Samanta, A., Zhu, Z.C., Myneni, R., 2013. Divergent Arctic-Boreal Vegetation Changes between North America and Eurasia over the Past 30 Years. Remote Sens. (Basel) 5 (5), 2093–2112.

Bongaarts, J., 2018. Special Report on Global Warming of 1.5 degrees C. The Federal Register/FIND 83 (7).

Brandt, M., et al., 2018. Satellite-Observed Major Greening and Biomass Increase in South China Karst During Recent Decade. Earth's Future 6 (7).

Cai, W., et al., 2014. Improved estimations of gross primary production using satellite-derived photosynthetically active radiation. J. Geophys. Res. Biogeo. 119 (1).

Cao, M.K., Prince, S.D., Small, J., Goetz, S.J., 2004. Remotely sensed interannual variations and trends in terestrial net primary productivity 1981–2000. Ecosystems 7 (3), 233–242.

Cao, Y., Song, Z., Wu, Z., Du, Z., 2022. Spatio-temporal dynamics of gross primary productivity in China from 1982 to 2017 based on different dataset. Chin. J. Appl. Ecol. 33 (10), 2644–2652.

Chen, M., et al., 2017a. Regional contribution to variability and trends of global gross primary productivity. Environ. Res. Lett. 12 (10).

Chen, T., et al., 2020. Unraveling the relative impacts of climate change and human activities on grassland productivity in Central Asia over last three decades. In: Science of the Total Environment, p. 743.

Chen, Y., et al., 2021. Accelerated increase in vegetation carbon sequestration in China after 2010: A turning point resulting from climate and human interaction. Glob. Chang. Biol. 27 (22), 5848–5864.

Chen, Z.S., Chen, Y.N., Bai, L., Xu, J.H., 2017b. Multiscale evolution of surface air temperature in the arid region of Northwest China and its linkages to ocean oscillations. Theor. Appl. Climatol. 128 (3–4), 945–958.

Chen, L., Liu, G., Feng, X., 2001. Estimation of Net Primary Productivity of Terrestrial Vegetation in China by Remote Sensing. Acta Botanica Sinica(11), 1191–1198.

Chenguang, T., et al., 2021. Projections of changes in ecosystem productivity under 1.5 °C and 2 °C global warming. Global Planet. Change 205.

Chuai, X., et al., 2020. Vegetation and climate zones based carbon use efficiency variation and the main determinants analysis in China. Ecol. Ind. 111 (C).

Committee, E., 2015. The 3rd National Assessment Report of Climatic Changes (in Chinese). Science Press, Beijing.

Cramer, W., et al., 2001. Global response of terrestrial ecosystem structure and function to CO_2 and climate change: results from six dynamic global vegetation models. Glob. Chang. Biol. 7 (4).

D'Odorico, P., Bhattachan, A., Davis, K.F., Ravi, S. and Runyan, C.W., 2013. Global desertification: Drivers and feedbacks. Advances in Water Resources, 51(Jan.).

Damm, A., et al., 2015. Far-red sun-induced chlorophyll fluorescence shows ecosystem-specific relationships to gross primary production: An assessment based on observational and modeling approaches. Remote Sens. Environ. 166.

de Jong, R., Verbesselt, J., Schaepman, M.E., de Bruin, S., 2012. Trend changes in global greening and browning: contribution of short-term trends to longer-term change. Glob. Chang. Biol. 18 (2), 642–655.

Deng, M., et al., 2022. The Response of Vegetation to Regional Climate Change on the Tibetan Plateau Based on Remote Sensing Products and the Dynamic Global Vegetation Model. Remote Sens. (Basel) 14 (14).

Ding, Y. et al., 2006. National Assessment Report of Climate Change (I): Climate Change in China and its future trend. Advances in Climate Change Research(01): 3-8+50.

Du, W., Sun, S., Wu, Y., Song, Z., 2020. The responses of gross primary production to drought in terrestrial ecosystems of China during 1980–2013. Chinese Journal of Ecology 39 (01), 23–35.

Fang, J., Ke, J., Tang, Z., Chen, A., 2001. Implications and estimations of four terrestrial productivity parameters. Journal of Plant Ecology(04), 414–419.

Farr, T.G., et al., 2007. The Shuttle Radar Topography Mission. Rev. Geophys. 45 (2).

Felton, A.J., Knapp, A.K., Smith, M.D., 2021. Precipitation-productivity relationships and the duration of precipitation anomalies: An underappreciated dimension of climate change. Glob. Chang. Biol. 27 (6), 1127–1140.

Feng, X., et al., 2007. Net primary productivity of China's terrestrial ecosystems from a process model driven by remote sensing. J. Environ. Manage. 85 (3).

Feng, Y., et al., 2019. Changes in the trends of vegetation net primary productivity in China between 1982 and 2015. Environ. Res. Lett. 14 (12).

Franzke, C.L.E., 2014. Warming trends nonlinear climate change. Nat. Clim. Chang. 4 (6), 423–424.

Fu, Y.L., et al., 2006. Depression of net ecosystem CO_2 exchange in semi-arid Leymus chinensis steppe and alpine shrub. Agric. For. Meteorol. 137 (3–4), 234–244.

Fu, G., Li, S.-W., Sun, W., Shen, Z.-X., 2016. Relationships Between Vegetation Carbon Use Efficiency and Climatic Factors on the Tibetan Plateau. Can. J. Remote. Sens. 42 (1).

Gang, C., et al., 2017. Modeling the dynamics of distribution, extent, and NPP of global terrestrial ecosystems in response to future climate change. Global Planet. Change 148.

Gao, Z.Q., Liu, J.Y., 2008. Comparative study on net productivity of vegetation in China. Chin. Sci. Bull. 53 (3), 317–326.

Guan, D.X., et al., 2006. CO2 fluxes over an old, temperate mixed forest in northeastern China. Agric. For. Meteorol. 137 (3–4), 138–149.

Hagen, S.C., et al., 2006. Statistical uncertainty of eddy flux-based estimates of gross ecosystem carbon exchange at Howland Forest. Maine. Journal of Geophysical Research-Atmospheres 111 (D8).

Hawinkel, P., et al., 2015. A time series processing tool to extract climate-driven interannual vegetation dynamics using Ensemble Empirical Mode Decomposition (EEMD). Remote Sens. Environ. 169, 375–389.

He, H., et al., 2019. Altered trends in carbon uptake in China's terrestrial ecosystems under the enhanced summer monsoon and warming hiatus. Natl. Sci. Rev. 6 (3), 505–514.

Hoerl, A.E., Kennard, R.W., 2012. Ridge Regression: Biased Estimation for Nonorthogonal Problems. Technometrics 12 (1).

Horvath, D.P., Anderson, J.V., Chao, W.S., Foley, M.E., 2003. Knowing when to grow: signals regulating bud dormancy. Trends Plant Sci. 8 (11).

Hou, J., Zhou, Y., Liu, Y., 2020. Spatial and Temporal Differences of GPP Simulated by Different Satellite-derived LAI in China. Remote Sensing Technology and Application 35 (05), 1015–1027.

Huang, N.E., et al., 1998. The Empirical Mode Decomposition and the Hilbert Spectrum for Nonlinear and Non-Stationary Time series Analysis. Proceedings: Mathematical, Physical and Engineering Sciences 454 (1971).

Huang, K., et al., 2018. Enhanced peak growth of global vegetation and its key mechanisms. Nat. Ecol. Evol. 2 (12), 1897–1905.

Hutchinson, M.F., 1995. Interpolating mean rainfall using thin plate smoothing splines. Int. J. Geogr. Inf. Syst. 9 (4), 385–403.

Ichii, K., et al., 2017. New data-driven estimation of terrestrial CO_2 fluxes in Asia using a standardized database of eddy covariance measurements, remote sensing data, and support vector regression. Journal of Geophysical Research-Biogeosciences 122 (4), 767–795.

Ji, F., Wu, Z., Huang, J., Chassignet, E.P., 2014. Evolution of land surface air temperature trend. Nat. Clim. Chang. 4 (6).

Jia, B., et al., 2020. Impacts of land use change and elevated CO_2 on the interannual variations and seasonal cycles of gross primary productivity in China. Earth Syst. Dyn. 11 (1).

Jiao, W., et al., 2017. Inversion of net primary productivity in the arid region of Northwest China based on various regressions. Resources Science 39 (03), 545–556.

Jiao, K., Gao, J., Wu, S., Hou, W., 2018. Research progress on the response processes of vegetation activity to climate change. Acta Ecol. Sin. 38 (06), 2229–2238.

Jiao, K., Gao, J., Wu, S., 2019. Climatic determinants impacting the distribution of greenness in China: regional differentiation and spatial variability. Int. J. Biometeorol. 63 (4).

Jiao, F., Liu, H., Xu, X., Gong, H., Lin, Z., 2020. Trend Evolution of Vegetation Phenology in China during the Period of 1981–2016. Remote Sens. (Basel) 12 (3).

Jing, Y., Zhu, H., Bi, R., Hou, M., 2021. Using temporal and spatial scales to unravel the effects of climatic factors on vegetation variations in China. Front. Ecol. Evol. 9 (November), 1–11.

Jung, M., et al., 2011. Global patterns of land-atmosphere fluxes of carbon dioxide, latent heat, and sensible heat derived from eddy covariance, satellite, and meteorological observations. Journal of Geophysical Research-Biogeosciences 116.

Kang, W., Wang, T., Liu, S., 2018. The Response of Vegetation Phenology and Productivity to Drought in Semi-Arid Regions of Northern China. Remote Sens. (Basel) 10 (5).

Keenan, T.F., Riley, W.J., 2018. Greening of the land surface in the world's cold regions consistent with recent warming. Nat. Clim. Chang. 8 (9).

Körner, C., 2015. Paradigm shift in plant growth control. Curr. Opin. Plant Biol. 25.

Lehouerou, H.N., 1984. Rain use efficiency-a unifying concept in arid-land ecology. J. Arid Environ. 7 (3), 213–247.

Li, C., et al., 2008. The design and applicatiob of CO_2 Flux data processing system at ChinaFLUX. GEO-INFORMATION SCIENCE(05), 557–565.

Li, X., et al., 2013. Estimation of gross primary production over the terrestrial ecosystems in China. Ecol. Model. 261–262.

Li, W., et al., 2018. Recent changes in global photosynthesis and terrestrial ecosystem respiration constrained from multiple observations. Geophys. Res. Lett. 45 (2).

Li, Y., Huang, M., Ji, J., Gong, H., 2015. Studies on the response mechanisms of vegetation net primary productivity in Chinese monsoon region to the variations of East Asian summer monsoon. Climatic and Environmental Research 20 (05), 544–554.

Li, X., Xiao, J., 2019. Mapping Photosynthesis Solely from Solar-Induced Chlorophyll Fluorescence: A Global, Fine-Resolution Dataset of Gross Primary Production Derived from OCO-2. Remote Sens. (Basel) 11 (21).
Li, Y.Z., Zhang, Y., Lv, J., 2022. Interannual variations in GPP in forest ecosystems in Southwest China and regional differences in the climatic contributions. Eco. Inform. 69.
Li, X.R., Zhu, Z.C., Zeng, H., Piao, S.L., 2016. Estimation of gross primary production in China (1982–2010) with multiple ecosystem models. Ecol. Model. 324, 33–44.
Li, Y., 2021. The response of gross primary production to the summer monsoon climate change over easern China, Institute of Geographical Sciences and Resources, Chinese Academy of Sciences, Beijing, 77-78 pp.
Liu, M., et al., 2012. Uncertainty analysis in data processing on the estimation of net carbon exchanges at different forest ecosystems in China. J. For. Res. 17 (3), 312–322.
Liu, Y., 2013. The Spatial and Temporal Variations of Water Use Efficiency in China's Terrestrial Ecosystems Simulated Using Remote Sensing and a Process-based Model. Nanjing University.
Liu, Q., et al., 2017b. Ability of sun-induced chlorophyll fluorescence on estimating terrestrial ecosystem gross primary productivity in China. Remote Sensing Technology and Application 32 (02), 363–373.
Liu, Y., Liu, H., Chen, Y., Gang, C., Shen, Y., 2022. Quantifying the contributions of climate change and human activities to vegetation dynamic in China based on multiple indices. Sci. Total Environ. 838 (P4).
Liu, H., Zhang, M., Lin, Z., 2017a. Relative importance of climate changes at different time scales on net primary productivity-a case study of the Karst area of northwest Guangxi. China. Environmental Monitoring and Assessment 189 (11).
Liu, H., Zhang, M., Lin, Z., Xu, X., 2018. Spatial heterogeneity of the relationship between vegetation dynamics and climate change and their driving forces at multiple time scales in Southwest China. Agric. For. Meterol. 256–257.
Liu, H., Zhan, Q., Yang, C., Wang, J., 2019. The multi-timescale temporal patterns and dynamics of land surface temperature using Ensemble Empirical Mode Decomposition. Sci. Total Environ. 652, 243–255.
Lu, X., et al., 2018. Seasonal patterns of canopy photosynthesis captured by remotely sensed sun-induced fluorescence and vegetation indexes in mid-to-high latitude forests: A cross-platform comparison. Sci. Total Environ. 644.
Lucht, W., et al., 2002. Climatic control of the high-latitude vegetation greening trend and Pinatubo effect. Science 296 (5573), 1687–1689.
Ma, J., et al., 2019. Trends and controls of terrestrial gross primary productivity of China during 2000–2016. Environ. Res. Lett. 14 (8).
Myers-Smith, I.H., et al., 2020. Complexity revealed in the greening of the Arctic. Nat. Clim. Chang. 10 (2), 106–117.
Myneni, R., Y. Knyazikhin, T. Park, 2015. MOD15A2H MODIS/Terra Leaf Area Index/ FPAR 8-Day L4 Global 500m SIN Grid V006. NASA EOSDIS Land Processes DAAC.
Myneni, R.B., Keeling, C.D., Tucker, C.J., Asrar, G., Nemani, R.R., 1997. Increased plant growth in the northern high latitudes from 1981 to 1991. Nature 386 (6626), 698–702.
Nemani, R.R., et al., 2003. Climate-Driven Increases in Global Terrestrial Net Primary Production from 1982 to 1999. Science 300 (5625).
Nima, M., et al., 2020. Recent amplified global gross primary productivity due to temperature increase is offset by reduced productivity due to water constraints. AGU Advances 1 (4).
Noora, S., 2020. Detecting Multicollinearity in Regression Analysis. Am. J. Appl. Math. Stat. 8 (2).
O, R.F.A., M, S.S. and Y, W., 2021. Restricted Ridge Regression estimator as a parameter estimation in multiple linear regression model for multicollinearity case. Journal of Physics: Conference Series, 1725(1).
Ouyang, X., et al., 2021. Applying a projection pursuit model for evaluation of ecological quality in Jiangxi Province. China. Ecological Indicators 133, 108414.
Pan, N., et al., 2018. Increasing global vegetation browning hidden in overall vegetation greening: Insights from time-varying trends. Remote Sens. Environ. 214, 59–72.
Piao, S., et al., 2005. Changes in vegetation net primary productivity from 1982 to 1999 in China. Global Biogeochem. Cycles 19 (2).
Piao, S.L., et al., 2014. Evidence for a weakening relationship between interannual temperature variability and northern vegetation activity. Nature. Communications 5.
Piao, S.L., et al., 2017. Weakening temperature control on the interannual variations of spring carbon uptake across northern lands. Nature. Clim. Change 7 (5), 359-+.
Pinzon, J.E., Tucker, C.J., 2014. A Non-Stationary 1981–2012 AVHRR NDVI3g Time Series. Remote Sens. (Basel) 6 (8).
Qian, Q., et al., 2022. Improving herders' income through alpine grassland husbandry on Qinghai-Tibetan Plateau. Land Use Policy 113, 105896.
Qin, D., et al., 2005. Assessment of Climate and Environmental Evolution in China (I): Climate and Environmental Change and Future Trends in China. Advances. Clim. Change Research(01), 4–9.
Qiu, K., 2015. Estimating regional vegetation gross primary producitivity, evapotranspiration, water use efficiency and their spatial and temporal distribution across China. Beijing Forestry University.
Qiu, R., et al., 2020. A Comparison of OCO-2 SIF, MODIS GPP, and GOSIF Data from Gross Primary Production (GPP) Estimation and Seasonal Cycles in North America. Remote Sens. (Basel) 12 (2).
Rossini, M., et al., 2015. Red and far red Sun-induced chlorophyll fluorescence as a measure of plant photosynthesis. Geophys. Res. Lett. 42 (6).
Running, S., et al., 2004. A Continuous Satellite-Derived Measure of Global Terrestrial Primary Production. Bioscience 54 (6).
Running, S.W. and Zhao, M., 2019. Daily GPP and Annual NPP (MOD17A2H/A3H) and Year-end GapFilled (MOD17A2HGF/A3HGF) Products NASA Earth Observing System MODIS Land Algorithm (For Collection 6).
Running, S.W., Nemani, R., Glassy, J.M. and Thornton, P.E., 1999. MODIS DAILY PHOTOSYNTHESIS (PSN) AND ANNUAL NET PRIMARY PRODUCTION (NPP) PRODUCT(MOD17), Algorithm Theoretical Basis Document.
Saatchi, S., et al., 2013. Persistent effects of a severe drought on Amazonian forest canopy. PNAS 110 (2), 565–570.
Schuur, E.A.G., Chadwick, O.A., Matson, P.A., 2001. Carbon Cycling and Soil Carbon Storage in Mesic to Wet Hawaiian Montane Forests. Ecology 82 (11).
Shangguan, W., Dai, Y., Duan, Q., Liu, B., Yuan, H., 2014. A global soil data set for earth system modeling. J. Adv. Model. Earth Syst. 6 (1), 249–263.
Shen, M., et al., 2016. Strong impacts of daily minimum temperature on the green-up date and summer greenness of the Tibetan Plateau. Glob. Chang. Biol. 22 (9), 3057–3066.
Shi, S., et al., 2021. Quantitative contributions of climate change and human activities to vegetation changes over multiple time scales on the Loess Plateau. Sci. Total Environ. 755 (prepublish).
Soner, Ç., Samet, E., Hasan, A.S., 2019. Comparison of Least Squares, Ridge Regression and Principal Component Approaches in the Presence of Multicollinearity in Regression Analysis. Turkish Journal of Agriculture - Food Science and Technology 7 (8).
Stephen, D.G., et al., 2008. Global potential net primary production predicted from vegetation class, precipitation, and temperature. Ecology 89 (8).
Sun, Q., et al., 2017. A systematic review of research studies on the estimation of net primary productivity in the Three-River Headwater Region. China Journal of Geographical Sciences 27 (02), 161–182.
Sun, R., Chen, S., Su, H., 2021. Climate Dynamics of the Spatiotemporal Changes of Vegetation NDVI in Northern China from 1982 to 2015. Remote Sens. (Basel) 13 (2).
Tao, B., Li, K., Shao, X., Cao, M., 2003. The temporal and spatial patterns of terrestrial net primary productivity in China. J. Geog. Sci. 13 (2).
Turner, D.P., et al., 2006. Evaluation of MODIS NPP and GPP products across multiple biomes. Remote Sens. Environ. 102 (3).
Tzuk, O., Ujjwal, S.R., Fernandez-Oto, C., Seifan, M., Meron, E., 2019. Interplay between exogenous and endogenous factors in seasonal vegetation oscillations. Sci. Rep. 9.
Vitasse, Y., Lenz, A. and Koerner, C., 2014. The interaction between freezing tolerance and phenology in temperate deciduous trees. Frontiers in Plant Science, 5.
Wan, G., Yang, M., Wang, X., 2012. Variations in soil temperature at BJ site on the central Tibetan Plateau. J. Mt. Sci. 9 (2).
Wang, J., et al., 2011a. Modelling carbon fluxes of different forests by coupling a remote-sensing model with an ecosystem process model. Int. J. Remote Sens. 32, 6539–6567.
Wang, J., et al., 2014. Comparison of Gross Primary Productivity Derived from GIMMS NDVI3g, GIMMS, and MODIS in Southeast Asia. Remote Sens. (Basel) 6 (3), 2108–2133.
Wang, J., et al., 2022a. Pixel-scale historical-baseline-based ecological quality: Measuring impacts from climate change and human activities from 2000 to 2018 in China. J. Environ. Manage. 313, 114944.
Wang, J. and Ye, H., 2021. Spatial interpolation dataset of 1km 8 days fine gridded meteorological observations in China in 2000 to 2018, National Ecological Science Data Center.
Wang, X., Hou, J., He, N., 2023. Distribution pattern and driving factors of plant community productivity from east to west in China. Acta Ecol. Sin. 43 (06), 2488–2500.
Wang, T., Song, X., Yan, C., Li, S., Xie, J., 2011b. Remote sensing analysis on aeolian desertification trends in northern China during 1975–2010. J. Desert Res. 31 (06), 1351–1356.
Wang, J., Wang, J., Ye, H., Liu, Y., He, H., 2017a. An interpolated temperature and precipitation dataset at 1-km grid resolution in China (2000–2012). China Scientific Data 2 (1), 88–95.
Wang, Y., Xie, Z., Jia, B., Yu, Y., 2015b. imulation and evaluation of gross primary productivity in China by using land surface model CLM4. Clim. Environ. Res. 20 (01), 97–110.
Wang, J., Yang, Y., Zuo, C., Gu, F., He, H., 2021. Impacts of human activities and climate change on gross primary productivity of the terrestrial ecosystems in China. Acta Ecol. Sin. 41 (18), 7085–7099.
Wang, T., Yang, D., Zheng, G., Shi, R., 2022b. Possible negative effects of earlier thaw onset and longer thaw duration on vegetation greenness over the Tibetan Plateau. Agric. For. Meteorol. 326.
Wang, Q., Zheng, H., Zhu, X., Yu, G., 2015a. Primary estimation of Chinese terrestrial carbon sequestration during 2001–2010. Science Bulletin 60 (6), 577–590.
Wang, Z., Zhong, J., Lan, H., Wang, Z., Sha, Z., 2017b. Association analysis between spatiotemporal variation of net primary productivity and its driving factors in inner mongolia, china during 1994–2013. Ecol. Ind. S1470160X17307380.
Wei, F.L., et al., 2018. Vegetation dynamic trends and the main drivers detected using the ensemble empirical mode decomposition method in East Africa. Land Degrad. Dev. 29 (8), 2542–2553.
Wen, X.F., et al., 2006. Soil moisture effect on the temperature dependence of ecosystem respiration in a subtropical Pinus plantation of southeastern China. Agric. For. Meteorol. 137 (3–4), 166–175.
Wen, Z., Wu, S., Chen, J., Lü, M., 2017. NDVI indicated long-term interannual changes in vegetation activities and their responses to climatic and anthropogenic factors in the Three Gorges Reservoir Region, China. Sci. Total Environ. 574, 947–959.
Wood, J.D., et al., 2017. Multiscale analyses of solar-induced florescence and gross primary production. Geophys. Res. Lett. 44 (1).
Wu, Z., Huang, N.E., 2009. Ensemble empirical mode decomposition : a noise-assisted data analysis method. Advances in Adaptive Data Analysis 1 (1).

Xiang, G., Xingxing, H., Kevin, L., Qianwen, D. and Ruiyang, W., 2021. Vegetation responses to climate change in the Qilian Mountain Nature Reserve, Northwest China. Global Ecology and Conservation, 28.
Xin, L., Binghao, J., Xin, L., 2020. Contributions of climate change, land use change and CO_2 to changes in the gross primary productivity of the Tibetan Plateau. Atmos. Oceanic Sci. Lett. 13 (1).
Xu, D.K., et al., 2019. Synchronous 500-year oscillations of monsoon climate and human activity in Northeast Asia. Nature. Communications 10.
Xu, Y., Xiao, F., Yu, L., 2020. Review of spatio-temporal distribution of net primary productity in forest ecosystem and its responses to climate change in China. Acta Ecol. Sin. 40 (14), 4710–4723.
Xue, Y., Zhang, B., He, C., Shao, R., 2019. Detecting Vegetation Variations and Main Drivers over the Agropastoral Ecotone of Northern China through the Ensemble Empirical Mode Decomposition Method. Remote Sens. (Basel) 11 (16).
Yan, H., et al., 2019. Multi-model analysis of climate impacts on plant photosynthesis in China during 2000–2015. Int. J. Climatol. 39 (15), 5539–5555.
Yang, K., et al., 2013. A multiscale soil moisture and freeze-thaw monitoring network on the third pole. Bull. Am. Meteorol. Soc. 94 (12), 1907–1916.
Yang, Y., Guan, H., Shen, M., Liang, W., Jiang, L., 2015. Changes in autumn vegetation dormancy onset date and the climate controls across temperate ecosystems in China from 1982 to 2010. Glob. Chang. Biol. 21 (2).
Yao, Y., et al., 2018. Spatiotemporal pattern of gross primary productivity and its covariation with climate in China over the last thirty years. Glob. Chang. Biol. 24 (1), 184–196.
Ye, Z., et al., 2019. Interannual and seasonal vegetation changes and influencing factors in the extra-high mountainous areas of southern Tibet. Remote Sens. (Basel) 11 (11).
Yin, Y., et al., 2017. Nonlinear variations of forest leaf area index over China during 1982–2010 based on EEMD method. Int. J. Biometeorol. 61 (6), 977–988.
Yu, G.R., et al., 2006. Overview of ChinaFLUX and evaluation of its eddy covariance measurement. Agric. For. Meteorol. 137 (3–4), 125–137.
Yu, G.R., et al., 2014. High carbon dioxide uptake by subtropical forest ecosystems in the East Asian monsoon region. PNAS 111 (13), 4910–4915.
Yuan, W., et al., 2010. Global estimates of evapotranspiration and gross primary production based on MODIS and global meteorology data. Remote Sens. Environ. 114 (7), 1416–1431.
Yuan, W., et al., 2019. Increased atmospheric vapor pressure deficit reduces global vegetation growth. Sci. Adv. 5 (8), 1–13.
Zan, M., et al., 2018. Performance of a two-leaf light use efficiency model for mapping gross primary productivity against remotely sensed sun-induced chlorophyll fluorescence data. Sci. Total Environ. 613–614.
Zhang, L., et al., 2019a. Carbon and water fluxes observed by the Chinese Flux Observation and Research Network (2003–2005). Science Data Bank 4 (01), 18–34.
Zhang, L., et al., 2019b. Interannual variability of terrestrial net ecosystem productivity over China: regional contributions and climate attribution. Environ. Res. Lett. 14 (1).
Zhang, X., 2020. Response of different vegetation types to climate change and monsoon systems in Southwest China. Beijing Forestry University bachelor's degree Thesis.
Zhang, Y., Wang, J. and Watson, A.E., In review. Decadal climate change has shifted from a slowing to a sustained warming, causing vegetation to grow rapidly over the terrestrial ecosystems in China since 1980 to 2018. Science of the Total Environment.
Zhang, W., Wang, L., Xiang, F., Qin, W., Jiang, W., 2020. Vegetation dynamics and the relations with climate change at multiple time scales in the Yangtze River and Yellow River Basin, China. Ecol. Ind. 110 (C).
Zhang, X., Wang, H., Yan, H., Ai, J., 2021. Analysis of spatio-temporal changes of gross primary productivity in China from 2001 to 2018 based on Romote Sensing. Acta Ecol. Sin. 41 (16), 6351–6362.
Zhang, L., Wu, B., Li, X., Xing, Q., 2014. Classification system of China land cover for carbon budget. Acta Ecol. Sin. 34 (24), 7158–7166.
Zhao, M., Running, S.W., 2010. Drought-Induced Reduction in Global Terrestrial Net Primary Production from 2000 Through 2009. Science 329 (5994).
Zhao, M., Heinsch, F.A., Nemani, R.R., Running, S.W., 2004. Improvements of the MODIS terrestrial gross and net primary production global data set. Remote Sens. Environ. 95 (2).
Zhao, G., Ren, L., Ye, Z., 2022. Vegetation Dynamics in Response to Climate Change and Human Activities in a Typical Alpine Region in the Tibetan Plateau. Int. J. Environ. Res. Public Health 19 (19).
Zhou, L.M., et al., 2014. Widespread decline of Congo rainforest greenness in the past decade. Nature 509 (7498), 86-+.
Zhou, Y., et al., 2020. Modeling the Effects of Global and Diffuse Radiation on Terrestrial Gross Primary Productivity in China Based on a Two-Leaf Light Use Efficiency Model. Remote Sens. (Basel) 12 (20).
Zhou, Y.-Z., Jia, G.S., 2016. Precipitation as a control of vegetation phenology for temperate steppes in China. Atmos. Oceanic Sci. Lett. 9 (03), 162–168.
Zhou, T., Zhang, L., Li, H., 2008. Changes in global land monsoon area and total rainfall accumulation over the last half century. Geophys. Res. Lett. 35 (16).
Zhu, X.-J., et al., 2014. Geographical statistical assessments of carbon fluxes in terrestrial ecosystems of China: Results from upscaling network observations. Global Planet. Change 118, 52–61.
Zhu, W., Pan, Y., Zhang, J., 2007. Estimation of net primary productivity of Chinese terrestrial vegetation based on remote sensing. J. Plant Ecol. 3, 413–424.
Zhu, H., Sun, R., Bi, R., Hou, M., 2022. Characterizing multiscale effects of climatic factors on the temporal variation of vegetation in different climatic regions of China. Theor. Appl. Climatol. 148 (1–2), 33–47.
Zhu, X., Zhang, S., Liu, T., Liu, Y., 2021. Impacts of heat and drought on gross primary productivity in China. Remote Sens. (Basel) 13 (3).